Smart Structures and Systems, *Vol. 33, No. 1 (2024) 1-16*
https://doi.org/10.12989/sss.2024.33.1.001

A real-time hybrid testing method for vehicle-bridge coupling systems

Guoshan Xu*[1,2,3], Yutong Jiang [1,2,3], Xizhan Ning [4] and Zhipeng Liu [1]

[1] *School of Civil Engineering, Harbin Institute of Technology, Harbin 150090, China*
[2] *Key Lab of Structures Dynamic Behavior and Control, Ministry of Education, Harbin Institute of Technology, Harbin 150090, China*
[3] *Key Lab of Intelligent Disaster Mitigation, Ministry of Industry and Information Technology, Harbin 150090, China*
[4] *College of Civil Engineering, Huaqiao University, Xiamen 361021, China*

(*Received January 26, 2023, Revised May 17, 2023, Accepted November 30, 2023*)

Abstract. The investigation on vehicle-bridge coupling system (VBCS) is crucial in bridge design, bridge condition evaluation, and vehicle overload control. A real-time hybrid testing (RTHT) method for VBCS (RTHT-VBCS) is proposed in this paper for accurately and economically disclosing the dynamic performance of VBCSs. In the proposed method, one of the carriages is chosen as the experimental substructure loaded by servo-hydraulic actuator loading system in the laboratory, and the remaining carriages as well as the bridge structure are chosen as the numerical substructure numerically simulated in one computer. The numerical substructure and the experimental substructure are synchronized at their coupling points in terms of force equilibrium and deformation compatibility. Compared to the traditional iteration experimental method and the numerical simulation method, the proposed RTHT-VBCS method could not only obtain the dynamic response of VBCS, but also economically analyze various working conditions. Firstly, the theory of RTHT-VBCS is proposed. Secondly, numerical models of VBCS for RTHT method are presented. Finally, the feasibility and accuracy of the RTHT-VBCS are preliminarily validated by real-time hybrid simulations (RTHSs). It is shown that, the proposed RTHT-VBCS is feasible and shows great advantages over the traditional methods, and the proposed models can effectively represent the VBCS for RTHT method in terms of the force equilibrium and deformation compatibility at the coupling point. It is shown that the results of the single-degree-of-freedom model and the train vehicle model are match well with the referenced results. The RTHS results preliminarily prove the effectiveness and accuracy of the proposed RTHT-VBCS.

Keywords: hybrid simulation; numerical model; real-time hybrid simulation; real-time hybrid testing method; vehicle-bridge coupling system

1. Introduction

1.1 Background and motivation

The investigation on vehicle-bridge coupling system (VBCS) plays an important role in bridge design, bridge condition evaluation, and vehicle overload control. However, with the advancement of modern science and technology, bridge structure is developing toward the direction of economy, aesthetics, and diversification. At the same time, the load and speed of vehicles also increase with the increase in public transport demand. Therefore, describing the coupling dynamic characteristics of the VBCS could effectively provide technical support for the research of bridge dynamic characteristics and response. At present, vehicle models, bridge models and VBCS models have been proposed one after another for different bridges and vehicles. The common simplified vehicle models include single-degree-of-freedom vehicle model, double-degrees-of-freedom vehicle model (Tan and Uddin 2020, Muthalif *et al*. 2017), half vehicle model, and train vehicle model, etc. The common simplified bridge models are Bernoulli Euler beam element, quadrilateral Kirchhoff plate/shell element, and beam plate element in the finite element. The equation of motion for the vehicle bridge coupling vibration calculation model is usually solved iteratively through the above vehicle models and bridge models (Wang *et al*. 1992).

At present, a lot of research on VBCSs can be found, which can be divided into numerical simulation methods and traditional experimental methods. Numerical simulation is the most common research method for analyzing the various parameters of vehicles and bridges in which the simplified models are mostly used to carry out vibration analysis of VBCSs. Cai *et al*. (1996) adopted the moving load-track beam model and two-degrees-of-freedom secondary suspension system respectively to study the VBCS. Lee *et al*. (2009) simplified vehicles as a five-degrees-of-freedom model with active controller and studied the influence of structural parameters on VBCS. Min *et al*. (2017) modeled maglev vehicle as a three-dimensional model with one body and four bogies, and studied the transverse resonance of maglev vehicle. However, the simplified vehicle model is sometimes too subjective to realistically consider characteristics of vehicle nonlinearity and randomness. Therefore, numerical simulation methods are more suitable for the preliminary analysis of VBCS, and it is impossible to explore the

*Corresponding author, Ph.D., Associate Professor,
E-mail: xuguoshan@hit.edu.cn

ISSN: 1738-1584 (Print), 1738-1991 (Online)

vehicle-bridge interaction mechanism and bridge dynamic characteristics in depth.

The traditional experimental methods include the road spectrum iteration method and the indirect measurement method of mobile vehicles (Yang *et al*. 2004). The road spectrum iteration method is to collect strain, acceleration, force, and other information when the vehicle is driving on the road, and uses the actuators to load the collected information to reproduce the real force situation of the vehicle. Shi *et al*. (2010) analyzed the principle of remote parameter control and the test method of road simulator, and the road simulation test of motorcycle was implemented with road simulator produced by MTS company. Meng *et al*. (2019) proposed a new method for assessing the bridge conditions based on nonlinear vibration analysis. Duvnjak *et al*. (2020) used diagnostic load testing to assess the condition of existing bridges. Xi *et al*. (2017) analyzed the performance of a real-time BeiDou Navigation Satellite System to determine the deformations and vibration of a cable-stayed bridge in Wuhan, which proved that the BeiDou Navigation Satellite System can provide high-precision deflection and accurate modal frequency information in real-time bridge deformation monitoring. However, the road spectrum iteration method is too time-consuming and labor-intensive and requires a targeted experimental design scheme, which is not highly applicable. The indirect measurement method could not reflect the time-variability.

In order to solve the adverse effects of numerical simulation methods and traditional experimental methods, real-time hybrid testing (RTHT) method has emerged and developed in the field of earthquake engineering (Nakashima *et al*. 1992, Nakashima and Masaoka 1999, Schellenberg *et al*. 2009a, b). The RTHT method (Mahmoud *et al*. 2013, Yang *et al*. 2009, Castaneda *et al*. 2012, Shao *et al*. 2016, Chen and Chen 2020) divides the research object into the numerical substructure and experimental substructure. The numerical substructure is the part of the structure with relatively simple dynamic performance, which is simulated and analyzed by a computer. The experimental substructure is the part with relatively complex dynamic performance, which is tested in the laboratory. Therefore, it could not only save time and money, but also facilitates the completion of various target scheme for the research subjects. The RTHT method has high requirements for the numerical integration algorithms and the loading systems. On the one hand, the numerical integration algorithm can be divided into explicit and implicit methods according to whether the reaction of the current integration step can be represented by the reaction of the previous integration step. The common explicit integration algorithms include central difference method (Wu *et al*. 2009), Newmark-βmethod, OS method (Wu *et al*. 2006), CR method (Chen *et al*. 2012a), equivalent force control method, and so on. Xu *et al*. (2020, 2022) proposed an explicit central difference method (CDM) and a three-variable control method with velocity positive feedback to improve the experimental accuracy and stability of shaking table substructure testing. Wu *et al*. (2006) assumed the speed based on the operating-splitting method, analyzed its stability, and applied this method to the real-time hybrid test. The equivalent force control method was proposed for solving the nonlinear equations of motion with implicit step-by-step integration algorithms (Wu *et al*. 2007). Guo *et al*. (2021) proposed one moving load convolution integral method for the real-time calculation of the track-bridge structure dynamics independent of the numerical model. Guo *et al*. (2022) proposed an off-line hybrid simulation method on train-track-bridge coupling vibration in high-speed railway combined with the fixed-point interaction algorithm.

On the other hand, since the dynamic characteristics, calculations, and communication delays of the actuator cause changes in signal phase and amplitude, reasonable time delay compensation is required. In order to improve the boundary condition simulation ability of the loading system and reduce the adverse effects of the time delay on the accuracy and stability of RTHT method, scholars have conducted a lot of research on delay compensation. For example, model-based feed-forward feedback controller (Carrion *et al*. 2009), LQG controller (Phillips *et al*. 2014, Zhou *et al*. 2019), H_∞ controller (Ning *et al*. 2019, Ou *et al*. 2015), inverse control time delay compensation method (Chen *et al*. 2012b), self-adaptive control method (Ahmadizadeh *et al*. 2008, Wang *et al*. 2020, 2019), optimal discrete-time feedforward compensator (Hayati and Song 2017), and so on. Horiuchi *et al*. (1999) used polynomial linear extrapolation to compensate the time delay. Tang *et al*. (2023) proposed an offline shaking table hybrid test, which uses a combination of RTHT method and neural networks. Shao *et al*. (2021) proposed one adaptive compound control method which uses the adaptive state feedback control and interpolation prediction algorithm to compensate the time delay.

The RTHT method may be one available method for precisely disclosing the dynamic performance of VBCSs. However, the investigation on RTHT-VBCS has just started with few results and no real large-scale experimental verification. Some specific problems about RTHT method for VBCS deserve further investigation.

1.2 Scope

In recent years, the investigation on VBCSs usually adopts the numerical simulation methods and the traditional iteration experimental methods. For the numerical simulation methods, the simplified vehicle models are sometimes too subjective to realistically consider the characteristics of the vehicle nonlinearity and randomness, so as to the simulation results are less accurate. The shortcoming of the traditional iteration experimental methods includes high costs, could not reflect the time-variability, and could not guide the design of vehicle and bridge due to single working conditions. Therefore, this paper aims to propose one novel RTHT method for VBCS (RTHT-VBCS), for precisely and economically disclosing the dynamic characteristics of VBCSs. The proposed RTHT-VBCS can not only comprehensively consider the dynamic effect of external load on VBCS, but also economically carry out experimental investigation on

various working conditions by changing parameters of the bridges and vehicles.

The main contents of this study are as follows. The background, the motivation, and the scope are introduced in Section 1. The theory of the RTHT-VBCSs is proposed in Section 2. The numerical models of VBCS for RTHT method are presented in Section 3. The effectiveness and accuracy of the RTHT-VBCS are verified by real-time hybrid simulations (RTHSs) in Section 4. The conclusions are summarized in Section 5.

2. Theory of RTHT-VBCS

2.1 Principle of RTHT-VBCS

RTHT is a test method that combines the numerical calculation of the numerical substructure and the real-time loading of the experimental substructure. One typical VBCS with five carriages, as shown in Fig. 1, is used as an example to present the principle of the RTHT-VBCS in this paper. In the RTHT-VBCS, one of the carriages is chosen as the experimental substructure loaded by servo-hydraulic actuator loading system in the laboratory, and the remaining carriages as well as the bridge structure are chosen as the numerical substructure simulated in one computer. The numerical substructure and the experimental substructure are synchronized at their coupling points in terms of force equilibrium and deformation coordination.

The differential equation of motion for the vehicles in RTHT-VBCS is shown in Eq. (1).

$$\begin{aligned}&\mathbf{M}_N^B\mathbf{a}_{Ni}+\mathbf{C}_N^B\mathbf{v}_{Ni}+\mathbf{R}_N^B(\mathbf{y}_{Ni})+\mathbf{R}_N^V(\mathbf{y}_{Ni}^V,\mathbf{v}_{Ni}^V)\\&+\mathbf{R}_E^V(\mathbf{y}_{Ei}^V,\mathbf{v}_{Ei}^V,\mathbf{a}_{Ei}^V)=\mathbf{F}_i\end{aligned}\tag{1}$$

in which, superscript B represents the bridge, superscript V represents the vehicle, subscript N represents the numerical substructure and subscript E represents the experimental substructure, **M** is the mass matrix, **C** is thedamping matrix, **R** is the restoring force vector; **F** is the external excitation force input in VBCS; **y**, **v** and **a** are the displacement, velocity, and acceleration vector.

The principle of the RTHT-VBCS is shown in Fig. 1. In the RTHT-VBCS, the VBCS is divided into the numerical substructure and the experimental substructure, and the structural responses and the evaluation of structural performance can be obtained through both the real-time loading on specimen with the servo-hydraulic actuator loading system and the real-time calculating on the equation of motion of the numerical substructure. The dynamic characteristics of the vehicle part are relatively complex, which are loaded through servo-hydraulic actuators. However, the dynamic performance of the bridge part is relatively uncomplicated, which is chosen as the numerical substructure carrying out numerical simulation analysis. During the tests, these two substructures exchange signals in real-time to ensure the equilibrium and coordinate of the boundary conditions. Generally speaking, two degrees of freedom in both horizontal and vertical directions was considered between the vehicle and the bridge, and one degree of freedom in horizontal direction was considered between the carriage and the carriage.

As can be seen from Fig. 1, the principle of RTHT-VBCS consists of four parts, namely the vehicle experimental substructure, the numerical substructure, the controller, and the dynamic calculation system. The dynamic calculation system includes two parts, i.e., the bridge dynamics calculation system and the vehicle dynamics calculation system. The bridge dynamics calculation system calculates the coupling position $\boldsymbol{y}_{Ni}$ and velocity $\mathbf{v}_{Ni}$, and transmits them to the vehicle dynamics calculation system. The vehicle dynamics calculation system calculates the coupling force $\mathbf{R}_{Ni}^V$ and the vehicle displacement $\mathbf{y}_{Ni}^V$ at the coupling point and the

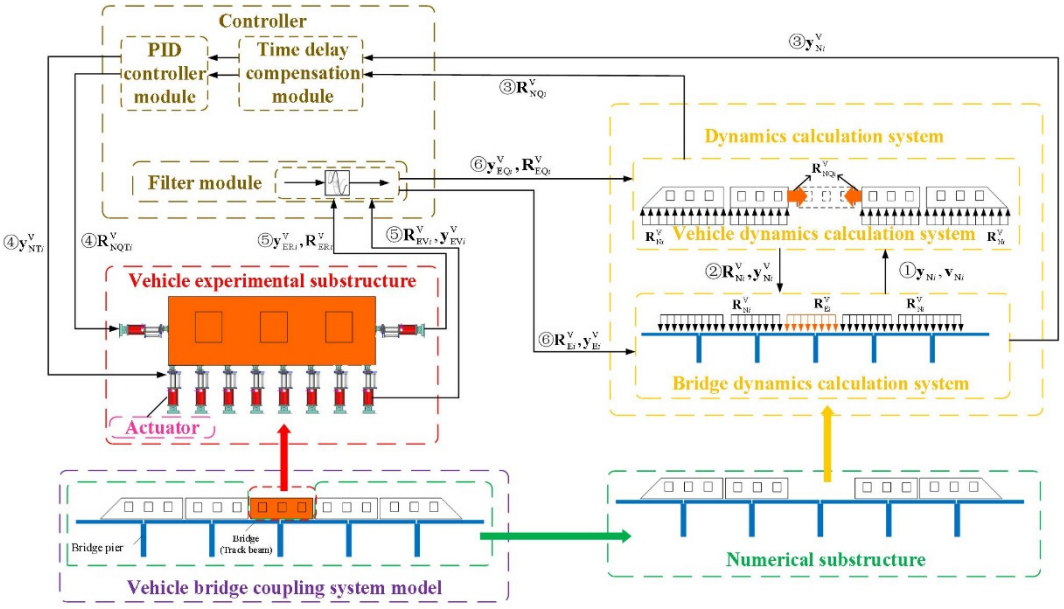

Fig. 1 The schematic diagram of the proposed RTHT-VBCS

traction force $\mathbf{R}_{NQi}^{V}$ between the carriages, and transmits $\mathbf{R}_{NQi}^{V}$ and $\mathbf{y}_{Ni}^{V}$ to the bridge dynamic calculation system. Then, the traction force $\mathbf{R}_{NQi}^{V}$ and the coupling displacement $\mathbf{y}_{Ni}^{V}$ were transmitted to the controller of servo-hydraulic actuators. The controller includes three parts, namely the PID controller module, the time delay compensation module, and the filter module. Through the time delay compensation and the PID controller, the servo-hydraulic actuators apply the vehicle displacement $\mathbf{y}_{\mathrm{NT}i}^{\mathrm{V}}$ and traction force $\mathbf{R}_{NQTi}^{V}$ to the vehicle experimental substructure respectively, and measures the experimental substructure horizontal displacement $\mathbf{y}_{ERi}^{V}$, horizontal coupling force $\mathbf{R}_{ERi}^{V}$, vertical displacement $\mathbf{y}_{EVi}^{V}$ and vertical coupling force $\mathbf{R}_{EVi}^{V}$ to realize the substructure boundary deformation compatibility. Through the filter, the horizontal displacement $\mathbf{y}_{EQi}^{V}$ and the horizontal force $\mathbf{R}_{EQi}^{V}$ are fed back to the vehicle dynamic calculation system, the coupling point displacement $\mathbf{y}_{Ei}^{V}$ and force $\mathbf{R}_{Ei}^{V}$ are fed back to the bridge dynamics calculation system to calculate the bridge deflection $\mathbf{y}_{Ni}$ and velocity $\mathbf{v}_{Ni}$, so as to realize the force equilibrium conditions. The vehicle dynamics calculation system calculates the coupling force $\mathbf{R}_{Ni}^{V}$ according to bridge deflection $\mathbf{y}_{Ni}$ and velocity $\mathbf{v}_{Ni}$, and so on until the vehicle has completely passed the bridge.

The implementation of the RTHT-VBCS is shown in Fig. 2. It should be mentioned that due to the dynamic characteristics of the current step of the numerical substructure is calculated by using the information of the previous integration step, it is more appropriate to choose the explicit integration algorithm.

The implementation of the RTHT-VBCS can be summarized as follows.

① Initialization of all parameters. The vehicle numerical substructure, the bridge numerical substructure, the integration algorithm, and the controller parameters are predetermined.

② Determine the initial coupling position $\mathbf{y}_{Ni}$ and coupling velocity $\mathbf{v}_{Ni}$ of the vehicle relative to the bridge.

③ The bridge numerical substructure calculates the coupling force $\mathbf{R}_{Ni}^{V}$ subjected to the dynamic responses of the vehicles.

④ The displacement $\mathbf{y}_{Ni}^{V}$ of the vehicle substructure at the coupling point is calculated by using the central difference method, and the traction force $\mathbf{R}_{NQi}^{V}$ between the carriages is calculated by the vehicle dynamics calculation system. Then, the displacement $\mathbf{y}_{Ni}^{V}$ and the traction force $\mathbf{R}_{NQi}^{V}$ are sent to the controller.

⑤ Through the time delay compensation module and the PID controller, the controller system transfers the vehicle displacement $\mathbf{y}_{NTi}^{V}$ and the traction force $\mathbf{R}_{NQTi}^{V}$ between the carriages to the servo-hydraulic actuators and loads the vehicle experimental substructure in a real-time mode, so that the vehicle experimental substructure and the numerical substructure realize the deformation coordination at the coupling site.

⑥ The data acquisition system measures the horizontal displacement $\mathbf{y}_{ERi}^{V}$ and force $\mathbf{R}_{ERi}^{V}$ of the vehicle, and the vertical displacement $\mathbf{y}_{EVi}^{V}$ and force $\mathbf{R}_{EVi}^{V}$ of the bridge through displacement transducers and force sensors.

⑦ Through the filter module, the controller transfers the horizontal displacement $\mathbf{y}_{EQi}^{V}$ and force $\mathbf{R}_{EQi}^{V}$ to the vehicle dynamics calculation system, the vehicle displacement $\mathbf{y}_{Ei}^{V}$ and force $\mathbf{R}_{Ei}^{V}$ to the bridge dynamic calculation system to calculate bridge deflection $\mathbf{y}_{Ni}$ and velocity $\mathbf{v}_{Ni}$. Then, calculates the coupling force $\mathbf{R}_{Ni}$ in the vehicle dynamics calculation system so as to the vehicle experimental substructure and the bridge numerical substructure can synchronized at their coupling points in terms of force balance and deformation coordination.

⑧ Go back to ②, and so on until the vehicle has completely passed the bridge.

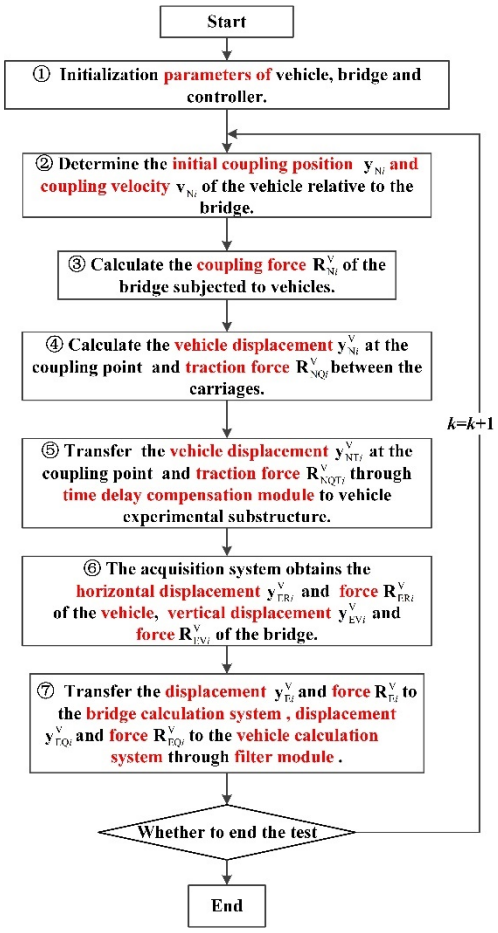

Fig. 2 The implementation of RTHT-VBCS

There are three main differences comparing with previous research on the RTHT-VBCS. The first one is that the proposed RTHT-VBCS method is a general method, that is, the vehicle model could be applied to single-degree-of-freedom vehicle model as well as train vehicle model. The second one is that the actuators are selected for loading

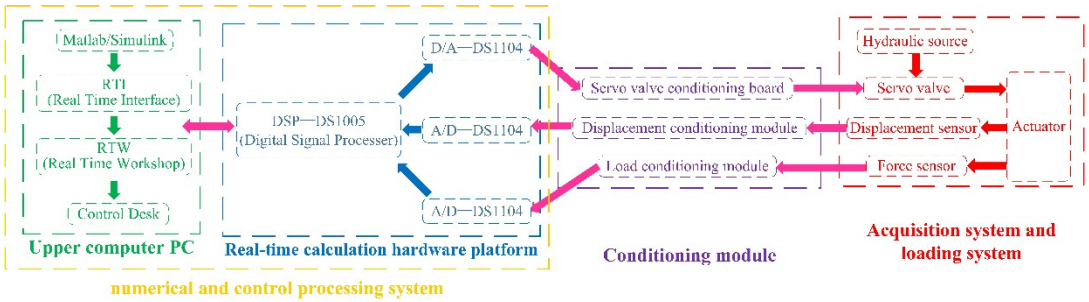

Fig. 3 The principle of RTHT-VBCS

instead of the shake table. The third one is that the central difference method is applied for solving the equation of motion in RTHT-VBCS.

Therefore, compared to the traditional iteration experimental method and the numerical simulation method, the RTHT-VBCS could not only accurately and effectively obtain the dynamic response of the VBCS, but also economically and precisely analyze various working conditions.

2.2 Test system of RTHT-VBCS

The hybrid test system of the RTHT-VBCS consists of the numerical and control processing system, the loading and acquisition system, and the conditioning system. The implementation test system is shown in Fig. 3. As can be seen in Fig. 3, the hybrid test system includes four parts, namely the upper computer PC, the real-time calculation hardware platform, the conditioning module, and the acquisition system and loading system. Upper computer PC consists of Matlab/Simulink program, RTI (Real Time Interface), RTW (Real Time Workshop), and Control Desk. RTI is the link between the real-time calculation hardware platform and Matlab/Simulink, which enables seamless automated download of real-time hardware code, control algorithm and simulation analysis. RTW provides a code generator which can easily and accurately convert Matlab/Simulink models into real-time codes. Control Desk is a comprehensive control platform for real-time simulation test, which enables the visual management, debugging and monitoring of system variables as well as the design of control algorithms. The real-time calculation hardware platform, e.g., DS1005 processor and I/O interface boards, can calculate the numerical models in real-time based on the measured data. The I/O interface board includes A/D and D/A. Generally speaking, the command displacements of the actuator are transmitted to the actuator through the D/A, whilst the displacement and force data measured from the sensors are fed back to the upper computer PC through the A/D. The conditioning module includes the servo valve conditioning board, the displacement conditioning module, and the load conditioning module, which converts the coordinates of the input into real inputs corresponding to the loading system. The acquisition system and loading system includes the hydraulic source, the servo valve, the displacement sensor, the force sensor, and the servo-hydraulic actuator, which is used to complete the test loading and data acquisition.

The implementation of the system is as follows. Firstly, builds the numerical and control processing system in the computer program, selects the appropriate I/O board, and sets the A/D and D/A gain control coefficients. Secondly, the program is compiled into hardware components through RTW/RTI. Finally, the displacement commands of servo-hydraulic actuator are calculated in real-time by the real-time calculation hardware platform and realized on the specimen. It should be mentioned that the whole process data is monitored and stored by the Control Desk. The Control Desk fully manages the process of the RTHS in terms of the hardware graphical settings, the variable control, and the parameter storage.

3. Numerical models for RTHT-VBCS

With the rapid development of computers and the continuous improvement of vibration theory, the numerical simulation methods could obtain simulation data under different working conditions. Compared to the numerical simulation methods, the RTHS is more suitable for investigating the VBCSs because that can not only carry out real large-scale physical tests on the complex vehicle structures, but also accurately simulate the bridge structures in computer. In RTHT-VBCS, the simplified numerical model of VBCS should be established so as to conduct in the real-time mode, which includes the vehicle model, the bridge model, and the pavement unevenness.

3.1 Vehicle model

(1) Single-degree-of-freedom vehicle model

The simplified single-degree-of-freedom vehicle model (Pawlus *et al.* 2011) is shown in Fig. 4. According to the D'Alembert principle, the equation of motion of the vehicle system is established as shown in Eq. (2).

$$m_s\ddot{y}_s + c_s(\dot{y}_s - \dot{y}_c) + k_s(y_s - y_c) = 0 \tag{2}$$

in which, m_s is the mass of the car body, c_s is the damping coefficient of the car body, k_s is the vertical body stiffness coefficient, y_s is the vertical displacement of the vehicle body, y_c is the vertical displacement of the contact point between wheel and bridge deck.

The force of vehicle on the bridge is composed of two

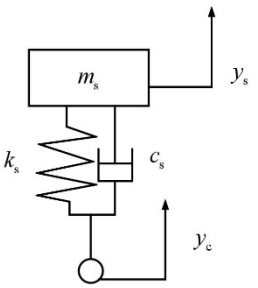

Fig. 4 Single-degree-of-freedom vehicle model

parts, namely the static load and the dynamic load. The static load is the gravity of the vehicle body in the simplified model, and the dynamic load mainly considers elastic force and damping force. Therefore, the force equation is shown in Eq. (3).

$$R_c(x,t) = m_s g + k_s(wy_s - y_c) + c_s(w\dot{y}_s - \dot{y}_c) \quad (3)$$

in which, w is the conversion coefficient.

(2) Train vehicle model

The train vehicle model, or named by sixteen-degrees-of-freedom vehicle model (Momoya *et al*. 2016) is shown in Fig. 5. Since the primary mass is simplified as a rigid body model, the forces will partially cancel with each other when establishing the motion equation. Therefore, the equations of motion for two-degrees-of-freedom rigid body model is shown in Eqs. (4)-(5).

$$\begin{aligned} &m_s g + k_s(wy_s - y_c) + c_s(w\dot{y}_s - \dot{y}_c)(3)m_s\ddot{y}_s \\ &+8c_{s1}\dot{y}_s - 2c_s\dot{y}_{p1} - 2c_s\dot{y}_{p2} - 2c_s\dot{y}_{p3} - 2c_s\dot{y}_{p4} \\ &+8k_s y_s - 2k_s y_{p1} - 2k_s y_{p2} - 2k_s y_{p3} - 2k_s y_{p4} = 0 \end{aligned} \quad (4)$$

$$\begin{aligned} &J_s\ddot{\alpha} + c_s\dot{\alpha}\sum_{i=1}^{8} l_{si}^2 - c_s\sum_{i=1}^{2} l_{si}\dot{y}_{p1} - c_s\dot{\beta}_1\sum_{i=1}^{2} l_{si}l_{sbi} \\ &-c_s\sum_{i=3}^{4} l_{si}\dot{y}_{p2} - c_s\dot{\beta}_2'\sum_{i=3}^{4} l_{si}l_{sbi} - c_s\sum_{i=5}^{6} l_{si}\dot{y}_{p3} \\ &-c_s\dot{\beta}_3\sum_{i=5}^{6} l_{si}l_{sbi} - c_s\sum_{i=7}^{8} l_{si}\dot{y}_{p4} - c_s\dot{\beta}_4\sum_{i=7}^{8} l_{si}l_{sbi} \\ &+k_s\alpha\sum_{i=1}^{8} l_{si}^2 - k_s\sum_{i=1}^{2} l_{si}y_{p1} - k_s\beta_1\sum_{i=1}^{2} l_{si}l_{sbi} \\ &-k_s\sum_{i=3}^{4} l_{si}y_{p2} - k_s\beta_2\sum_{i=3}^{4} l_{si}l_{sbi} - k_s\sum_{i=5}^{6} l_{si}y_{p3} \\ &-k_s\beta_3\sum_{i=5}^{6} l_{si}l_{sbi} - k_s\sum_{i=7}^{8} l_{si}y_{p4} - k_s\beta_4\sum_{i=7}^{8} l_{si}l_{sbi} = 0 \end{aligned} \quad (5)$$

in which, β is the turning angle of bogie around the centre of mass, l_{si} is the distance from the secondary suspension to the vehicle body centre of gravity, y_p is the primary suspension vertical displacement, y_c is the vertical displacement of the contact point between the wheel and the bridge deck, l_{pi} and l_{sbi} are the force arms of the primary and the secondary suspension to the bogie.

Therefore, the coupling force equation is shown in Eq. (6).

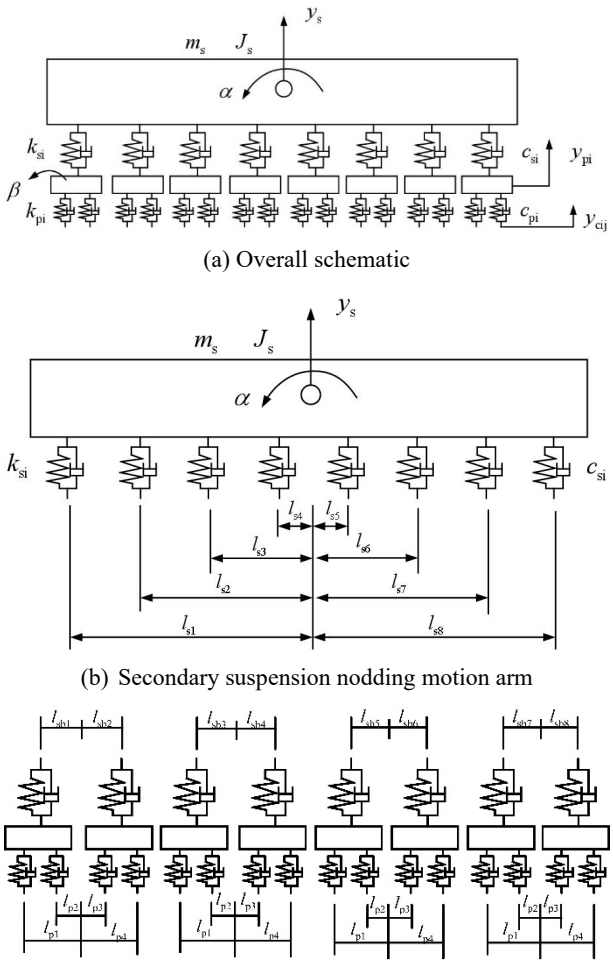

(a) Overall schematic

(b) Secondary suspension nodding motion arm

(c) Primary and secondary suspension points to bogie nodding motion arm

Fig. 5 Train vehicle model

$$\begin{aligned} R_c(x,t) = m_s g &+ k_p\left(\sum_{i=1}^{4}\sum_{j=1}^{4} wy_{pi} - y_{cij}\right) \\ &+ c_p\left(\sum_{i=1}^{4}\sum_{j=1}^{4} w\dot{y}_{pi} - \dot{y}_{cij}\right) \end{aligned} \quad (6)$$

in which, w is the conversion coefficient.

3.2 Bridge model

Generally speaking, the finite element method and the mode decomposition method are commonly used for analyzing the dynamic performance of the bridge. The finite element method can more accurately calculate the dynamic response of the vehicle at any position on the bridge. The mode decomposition method requires the corresponding coefficient matrix to be recalculated at each integral step, which inevitably reduces the computational efficiency. By comparing two methods, the finite element method is more suitable for analyzing the bridge. The process of the finite element method is as follows. Firstly, the bridge is divided into several discrete elements. Secondly, the force of each

element is analyzed and the vibration equation of the element is established. Finally, the dynamic response of the bridge is obtained by using the numerical integration method.

Specifically, the bridge structure can be simplified by plane finite element method, i.e., the multiple plane bar elements. Two nodes are calculated for each element, and each node has two-degrees-of-freedom. Therefore, the equation of motion for the bridge structure is established as follows.

$$\boldsymbol{M_B\ddot{X} + C_B\dot{X} + K_BX = Q^TR_c} \tag{7}$$

in which, subscript **B** means the bridge model, **X** is the displacement vector on each degree of freedom in the bridge model, $\dot{\mathbf{X}}$ and $\ddot{\mathbf{X}}$ are the velocity and acceleration vector, $\mathbf{R}_c$ is the coupling force vector, $\mathbf{Q^T}$ is the matrix of shape functions.

It should be noted that the finite element methods can be used to simulate the bridge models. For the proposed RTHT-VBCS method, there are two requirements if the finite element method is used to simulate the bridge models. On the one hand, the element can be calculated in real-time to obtain the accurate dynamic response of VBCS. On the other hand, the experimental substructure can be solved by the experimental element, that is, which can send the displacements and receive the forces at the coupling points between the vehicle and the bridge.

3.3 Pavement unevenness model

The smoothness of the pavement is an important indicator of road surface evaluation, which directly reflects the driving comfort and safety of the road surface. The harmonic superposition method is used for the simulation of the pavement unevenness in this paper. The central idea of this method is to superimpose series of sinusoidal curves with different wavelengths, amplitudes, and phase differences to realize the simulation of vector random processes and random fields. The essence of this method to simulate the pavement unevenness is to decompose and disperse the random pavement spectrum, thereby avoiding the limitation of spectral density function shape, which is relatively simple in the process of theoretical derivation and calculation.

Taking any point l_k on the pavement, and the random variable $x(l_k)$ corresponding to l_k. The triangular series expression of pavement roughness $x(l)$ is constructed by harmonic superposition method.

$$x(l) = \sum_{k=1}^{N} a_k \sin(2\pi n_k l + \varphi_k) \tag{8}$$

in which, l is the horizontal distance of the pavement, a_k is an independent random variable satisfying Gaussian distribution, φ_k is the independent random variable with equal probability in the range [0, 2π], and n_k indicates the central frequency of the kth interval after *N* equal parts.

The frequency range $[n_l, n_u]$ is divided into *N* equal parts as shown in the follows.

$$\Delta n = \frac{(n_u - n_l)}{N} \tag{9}$$

$$n_k = n_l + (k - 1/2)\Delta n \tag{10}$$

$$H_a(n_k) = H_a(n_0)\left(\frac{n_k}{n_0}\right)^{-\omega} \tag{11}$$

in which, n is the space frequency, n_l is the lower limit of spatial frequency, and the value is 0.01 m^{-1}, n_u is the upper limit of spatial frequency, e.g., the value is 2.83 m^{-1}, Δn is the internal width after *N* equal parts, n_k is the central frequency of the kth interval after *N* equal fractions, $H_a(n_k)$ is the spatial frequency power spectral density corresponding to the kth interval after *N* equal divisions, $H_a(n_0)$ is the spatial frequency power spectral density, n_0 is the spatial reference frequency, which the value is 0.1 m^{-1}, ω is the frequency index, and the value is usually 2.0.

When *N* is infinite, $a_k^2 = 2H_a(n_k)\Delta n$ could be obtained from Parseva equation, and the pavement roughness function *x*(*l*) can be converted to Eq. (12).

$$x(l) = \sum_{k=1}^{N} \sqrt{2H_a(n_k)\Delta n}\sin(2\pi n_k l + \varphi_k) \tag{12}$$

In case of the vehicle is driving on an uneven road at a uniform speed v, the pavement unevenness function is converted into a function of time, *i.e.*, $l = vt$ in Eq. (12).

In addition, according to the sampling theorem, $\Delta l \leq 1/(10n_u)$ (n_u = 2.83), then the minimum sampling time should meet the following conditions.

$$\Delta t \leq \frac{1}{10vn_u} \tag{13}$$

During the normal driving of vehicles on the bridge deck, it can be approximated that there is no separation between the vehicle and the bridge. The displacement coordinated condition between the vehicle and the bridge is the sum of the bridge vertical deformation and the unevenness of the bridge deck.

4. Hybrid simulation verification of RTHT-VBCS

4.1 Hybrid simulation scheme

The hybrid simulation schematic diagram of RTHT-VBCS is shown in Fig. 6. The Coupling displacement and velocity module is used to calculate the displacement and velocity at the coupling point of VBCS based on the dynamic response of the bridge and the relative position of the vehicle to the bridge at the present time. The Numerical vehicle model is the response calculation module of the numerical vehicle system under the action of displacement and velocity at the coupling point. The test vehicle model is the response calculation module of the experimental vehicle under the loading system model and the action of displacement and velocity at the coupling point. The Coupling force module is used to calculate the coupling

force of VBCS based on the dynamic response of the vehicles. The Bridge model is the dynamic response calculation module of the bridge under the action of coupling force. It should be mentioned that the loading system model is used to simulate the dynamic performance of the servo-hydraulic actuator loading system in the hybrid simulations in the simulations, while which is not necessary in actual RTHSs.

The solver ODE45 is used to solve the differential equations of motion for the numerical vehicle model, the numerical bridge model as well as the experimental vehicle model. The differential equation is solved by state-space method. The state-space equation is shown as follows.

$$\begin{aligned} \boldsymbol{x}_{n+1} &= \boldsymbol{A}\boldsymbol{x}_n + \boldsymbol{B}\boldsymbol{u}_n \\ \boldsymbol{y}_n &= \boldsymbol{C}\boldsymbol{x}_n + \boldsymbol{D}\boldsymbol{u}_n \end{aligned} \tag{14}$$

in which, $\boldsymbol{x}_n$ represents the state variable matrix, $\boldsymbol{u}_n$ represents the input variable matrix, $\boldsymbol{y}_n$ represents the output variable matrix, $\boldsymbol{A}$ represents the system matrix, $\boldsymbol{B}$ represents the input matrix, $\boldsymbol{C}$ represents the output matrix, $\boldsymbol{D}$ represents the feed-forward matrix.

The specific explanation of simulation notations in Fig. 6 are shown in Table 1.

The RTHT method requires real-time signal interaction between the numerical model and the experimental test. However, in the actual RTHT method, due to the time delay there is a certain error between the displacement command and the displacement response. In order to determine the impact of the time delay error on the test results, it is necessary to model the hardware system in the hybrid simulations. In this paper, one second-order transfer function proposed in literature (Wu *et al*. 2007) was selected to simulate the influence of the hardware system. The transfer function is shown in Eq. (15), which has been shown to be accurate enough to meet the hardware loading system requirements in RTHS. The transfer function model can reflect the performance of the loading control system, which indicates the hybrid simulation results based on the transfer function model could be approximately equal to the experimental results.

$$T(s) = \frac{\omega^2 e^{-\tau s}}{s^2 + 2\xi\omega s + \omega^2} \tag{15}$$

Table 1 Explanation of simulation notations

Module	Symbol	Definition
Coupling displacement and velocity module	location	relative position of the vehicle to bridge
	Xb	bridge substructure displacement at the coupling point
	Xg and Xg_	coupling point displacement
	Vg and Vg_	coupling point acceleration
	RT	time function
	XV_c	coupling point displacement and velocity.
	output	output
	Coupling pointa	coupling point acceleration
fcn	t	time
	y	relative position of the vehicle to bridge
Coupling force	RT	time fuction
	XV_c	coupling displacement and velocity.
	t	time
	Xt	experimental vehicle displacement
	F	coupling force in vehicle-bridge coupling system (static load and dynamic load)
	cpf	dynamic coupling force in VBCS (elastic force and damping force)
Separate	XV_c	coupling displacement and velocity
	XV_n	numerical vehicle displacement
	XV_p	experimental vehicle displacement
Merge1	t	time
	X0	numerical vehicle displacement and velocity
	X1	experimental vehicle displacement and velocity
	Xt	experimental vehicle displacement
	output	output
Merge	Xt	bridge substructure displacement at the coupling point
	output and output1	output

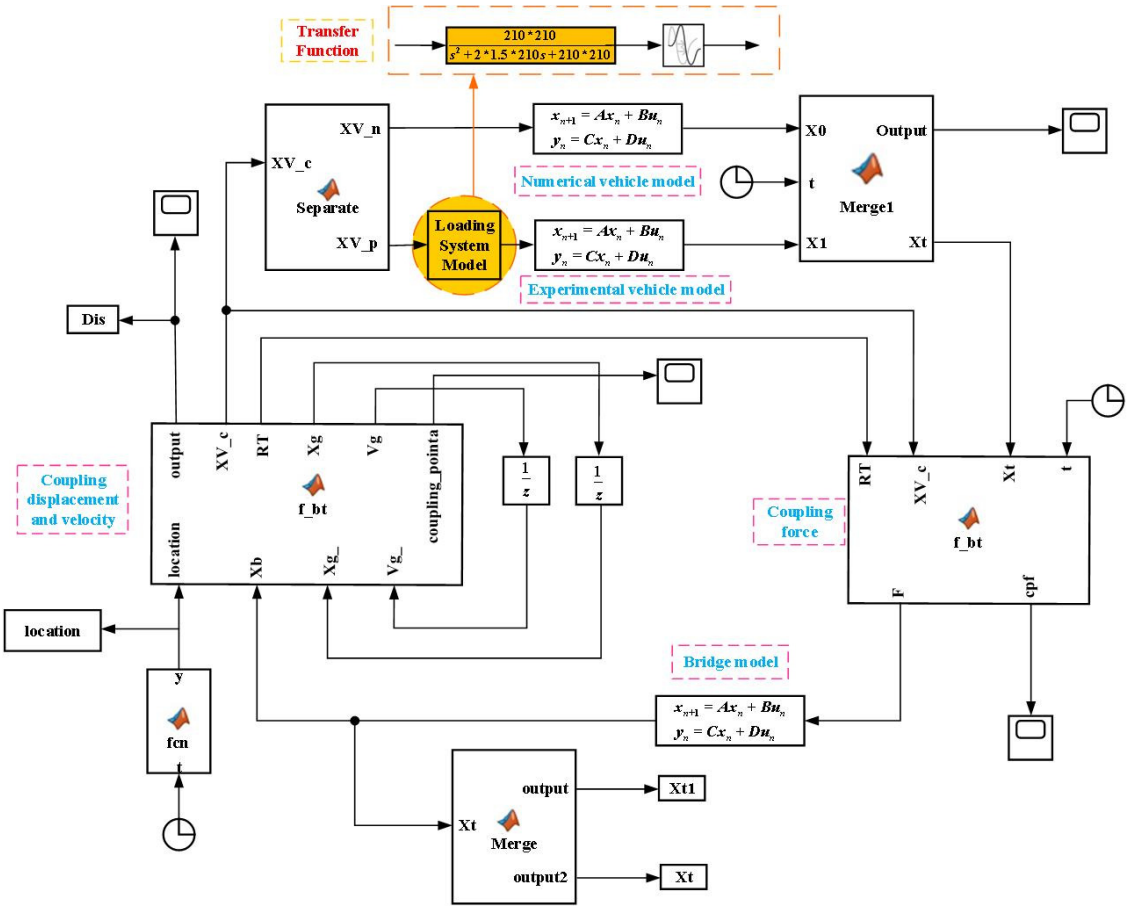

Fig. 6 The schematics diagram of RTHT-VBCS

in which, ξ is damping ratio of actuator, ω is circular frequency of actuator (rad/s), τ is pure time delay (s).

When ξ is 1.5, ω is 210 rad/s and τ is 0.0005 s, the displacement response of model under square wave command is shown in Fig. 7. It is shown that the responses follow the tracks of the commands well. The results show that the defined second-order transfer function model has reliable accuracy, which could appropriately reflect the performance of the loading control system in real-time hybrid testing method, and can be used for hybrid simulation research of the proposed RTHT-VBCS in this paper. The transfer function as shown in Eq. (15) is incorporated into the loading system module in Fig. 6, which has been marked by yellow.

The calculation parameters of the bridge are shown in Table 2. The schematic diagram of the bridge model is shown in Fig. 8. The bridge is simulated as a multi-span continuous Euler beam with simply supported ends in this study. Each span of Euler beam is divided into 50 elements, and the gap between the beams is 0.01 m. In this paper, the plane finite element only considers the vertical and out-of-plane rotation degrees of freedom and ignores the axial deformation, that means each node has two degrees of freedom.

The calculation parameters of the vehicle models consider two cases, i.e., Case 1 represents the single degree of freedom model and Case 2 represents the train vehicle model, as shown in Tables 3-4, respectively. In this paper, the central difference method is used to calculate the theoretical results with the same working conditions of two cases, which named by the Referenced results. And the corresponding results are compared with the hybrid simulation results of two cases to verify the effectiveness of the RTHT-VBCS. It should be mentioned that the number and orientation of actuators in RTHT-VBCS are different due to different vehicle model and different vehicle specimen. In Case 1, only one vertical actuator is used to emulate the boundary conditions in RTHT-VBCS. In Case

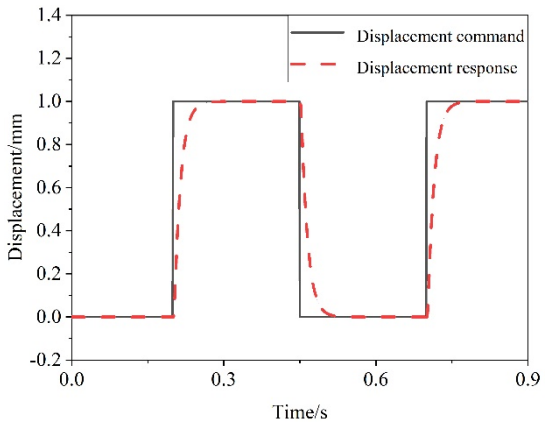

Fig. 7 Displacement response of actuator model under square wave command

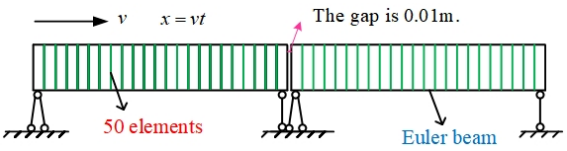

Fig. 8 The schematic diagram of the bridge model

Table 2 Calculation parameters of bridge model

Calculation span/m	Unit length mass/(kg/m^{-1})	Bending stiffness/(N·m^2)	Damping ratio
25	2303	8.323×10^9	0

Table 3 Calculation parameters of vehicle for Case 1

Project/unit	Data	Project/unit	Data
m_s/kg	5750	$v/(km\cdot h^{-1})$	100
$k_s/(N\cdot m^{-1})$	1.595 × 10^6	$c_s/(N\cdot s/m)$	0

2, eight vertical actuators and two horizontal actuators are used in order to meet the force equilibrium and deformation compatibility, as shown in Fig. 1.

In addition, in order to more accurately quantitative analysis the consistency between the hybrid simulation results and the referenced results, three aspects are used to comprehensively evaluate the error.

Firstly, the peak value error (PVE) is calculated by Eq. (16).

$$PVE = |(A - A_0)/A_0| \times 100\% \tag{16}$$

in which, A is the peak value of hybrid simulation results, A_0 is the peak value of the referenced results.

Secondly, the root mean square deviation (RMSD) is defined as follows.

$$RMSD = \sqrt{\frac{\sum_{i=1}^{N}\left(X_i^{\text{hybrid}} - X_i^{\text{referenced}}\right)^2}{\sum_{i=1}^{N}\left(X_i^{\text{referenced}}\right)^2}} \times 100\% \tag{17}$$

in which, X_i^{hybrid} is the peak value of hybrid simulation results, $X_i^{\text{referenced}}$ is the peak value of the referenced

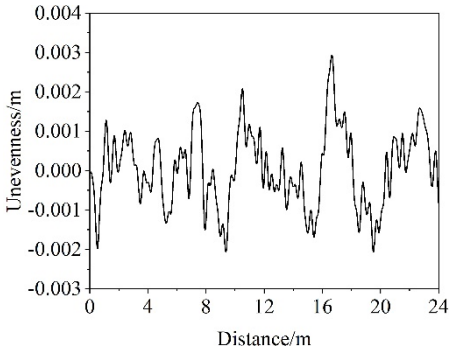

Fig. 9 Pavement unevenness of Class A

results. It can be seen from Eq. (17) that the RSMD represents the global evaluation of the error in the whole time. This error index can comprehensively reflect the influence of hardware equipment on the bridge mid span dynamic response. The smaller the RMSD is, the better the degree of coincidence is, the closer hybrid simulation results are to the referenced results.

Finally, the concept of correlation coefficient (CC) is used for evaluating the error. Assuming that the numerical simulation results and the referenced results over a period of time (T_1, T_2) are $X_i(T_1, T_2)$ and $Y_i(T_1, T_2)$ respectively, and the calculation formula is as follows.

$$CC = \frac{\sum_{i=T_1}^{T_2} X_i Y_i}{\left[\sum_{i=T_1}^{T_2} X_i^2 \sum_{i=T_1}^{T_2} Y_i^2\right]^{\frac{1}{2}}} \tag{18}$$

It should be noted that although the time delay compensation methods are not considered, the hybrid simulation results are almost consistent with the referenced results. The accuracy of the proposed method may be greatly improved by the delay compensation methods, *e.g.*, the polynomial interpolation method and the inverse transfer function method, while it is not the focus of the paper.

4.2 Result analysis

(1) Case 1

The pavement unevenness is taken as Class A. According to the section 3.3, when n_0 = 0.01 m^{-1}, n_l = 0.01 m^{-1}, n_u = 2.83 m^{-1}, l = 16 m, ω = 2, N = 1024, $H_a(n_0)$ = 10

Table 4 Calculation parameters of vehicle for Case 2

Project/unit	Data	Project/unit	Data	Project/unit	Data	Project/unit	Data
m_s/kg	44600	$c_s/(N\cdot s/m)$	4.6×10^3	l_{s6}/m	4.5	l_{s7}/m	7.5
m_p/kg	1200	$c_p/(N\cdot s/m)$	1.125 × 10^4	l_{s8}/m	10.5	l_{sb1}/m	-1.5
$J_s/(kg\cdot m^2)$	2.54 × 10^6	$J_p/(kg\cdot m^2)$	1535	l_{sb2}/m	-1.5	l_{sb3}/m	-1.5
$k_s/(N\cdot m^{-1})$	4.6 × 10^5	L/m	24×5	l_{sb4}/m	-1.5	l_{sb5}/m	1.5
$k_p/(N\cdot m^{-1})$	1.125 × 10^7	$v/(m\cdot s^{-1})$	160	l_{sb6}/m	1.5	l_{sb7}/m	1.5
Number of carriages	5	l_{s1}/m	-10.5	l_{sb8}/m	1.5	l_{p1}/m	-2.25
l_{s2}/m	-7.5	l_{s3}/m	-4.5	l_{p2}/m	-0.75	l_{p3}/m	0.75
l_{s4}/m	-1.5	l_{s5}/m	1.5	l_{p4}/m	2.25		

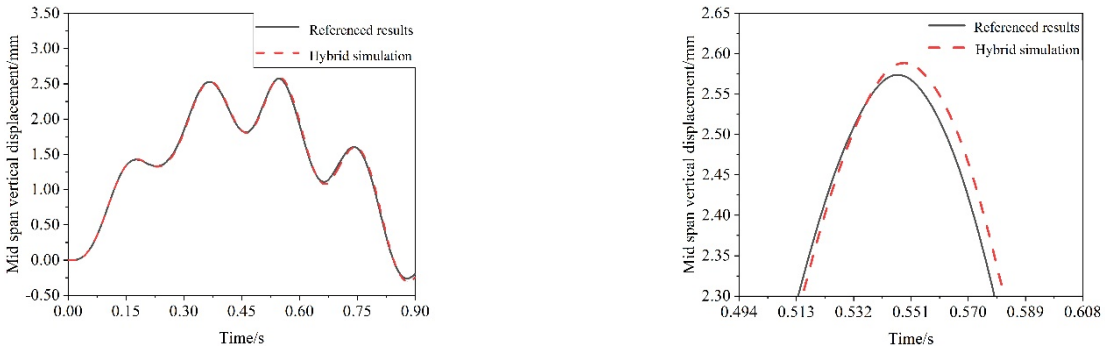

(a) Overall view (b) Close-up view

Fig. 10 Comparison of mid span displacement of the bridge for Case 1

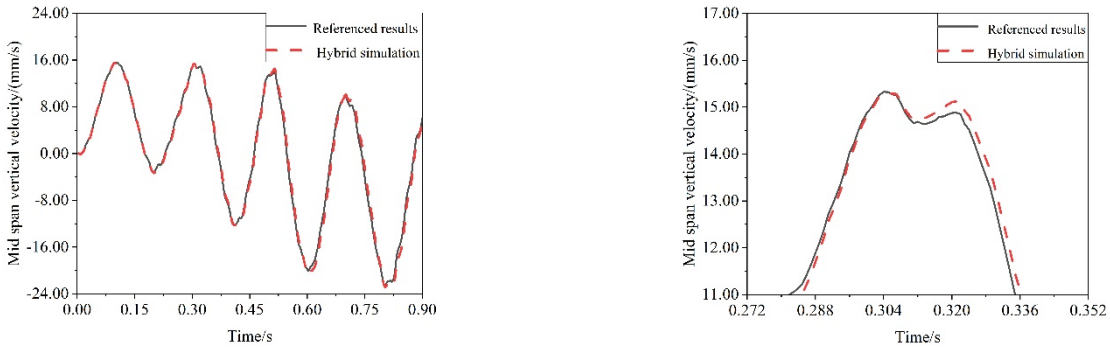

(a) Overall view (b) Close-up view

Fig. 11 Comparison of mid span displacement of the bridge for Case 1

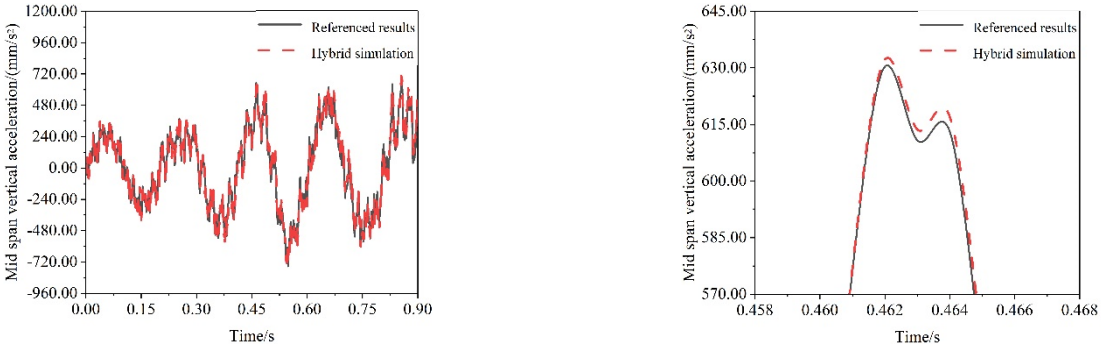

(a) Overall view (b) Close-up view

Fig. 12 Comparison of mid span acceleration of bridge for Case 1

$\times 10^{-6}$, the pavement unevenness of Class A can be obtained as shown in Fig. 9.

Then the hybrid simulation is carried out. The hybrid simulation results are compared with the corresponding referenced results under the same working conditions, as shown from Figs. 10-15. It is shown that the results of hybrid simulation match well with the referenced results for Case 1, e.g., the displacement, velocity, and acceleration of the bridge at the mid span and the servo-hydraulic actuator. The hybrid simulation results are evaluated through Eqs. (15)-(17), as shown in Table 5. It can be seen from Table 5 that the peak value errors, the root mean square deviations, and the correlation coefficients of dynamic that the peak value errors, the root mean square deviations, and the

Table 5 Hybrid simulation errors for Case 1

Calculation parameters		PVE	RMSD	CC
Mid span of bridge	Displacement	0.77%	1.67%	0.9999
	Velocity	1.82%	7.36%	0.9975
	Acceleration	0.32%	8.01%	0.9970
Actuator	Displacement	0.00%	1.05%	1.0000
	Velocity	2.00%	6.14%	0.9982
	Acceleration	0.25%	0.43%	1.0000

correlation coefficients of dynamic responses at the mid span of the bridge and actuator responses are less than 2%, less than 0.1, and more than 0.99, respectively. It shows that the results of the hybrid simulation are in good agreement with the referenced results.

As can be seen in Fig. 10 and Fig. 13, the error amplitude of mid span displacement of the bridge is 0.06 mm, and the error amplitude of the actuator displacement is 0.05 mm. These errors are mainly caused by the loading control errors of the actuator system, e.g., the amplitude error and the phase error. And the values of errors are small and acceptable for RTHS, which preliminarily proves the accuracy of the proposed method.

Based on the above analysis, it can be concluded that the calculation accuracy of the hybrid simulation program is reliable. Considering the simulation accuracy and test feasibility, the single degree of freedom vehicle model can be adopted for simulating the vehicle system in the RTHS.

(2) Case 2

When the simplified train vehicle model is used and ignores the pavement unevenness, the hybrid simulation results are shown in Figs. 16-19. It is shown that the results of hybrid simulation almost match the referenced results for Case 2, e.g., the displacement responses at mid span of bridge, the vertical displacements at the first coupling point, the vertical displacements of vehicle body, and the bogie displacements. The calculation parameters of the bridge and

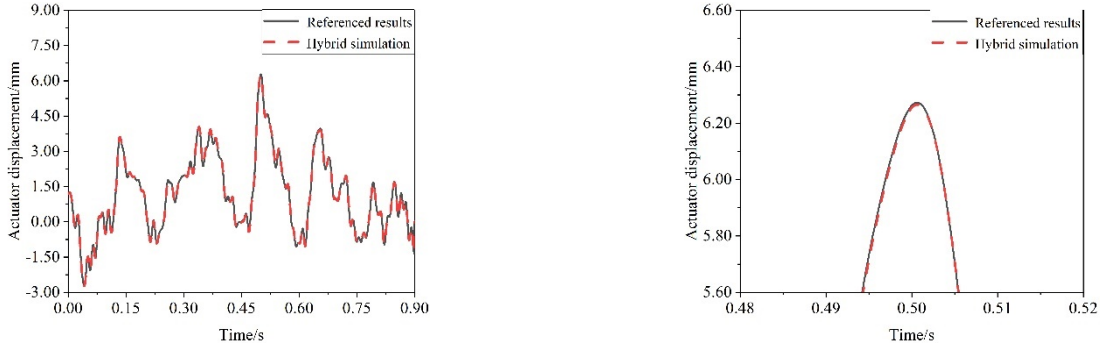

(a) Overall view (b) Close-up view

Fig. 13 Comparison of actuator displacement for Case 1

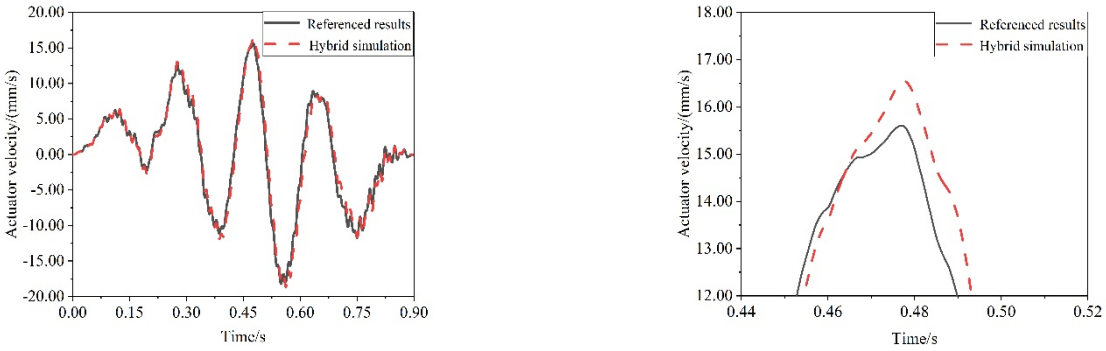

(a) Overall view (b) Close-up view

Fig. 14 Comparison of actuator velocity for Case 1

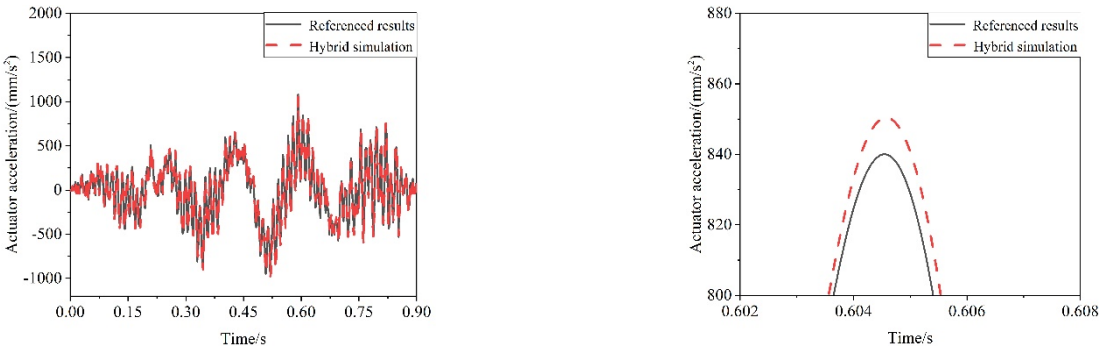

(a) Overall view (b) Close-up view

Fig. 15 Comparison of actuator acceleration for Case 1

Table 6 Hybrid simulation errors for Case 2

Calculation parameters	PVE	RMSD	CC
Mid span displacement	24.20%	23.50%	0.9721
Vertical displacement at the first coupling point	7.69%	7.77%	0.9987
Vehicle body displacement	18.21%	18.78%	0.9980
Bogie displacement	16.04%	30.31%	0.9566

vehicle are shown in Table 2 and Table 4. The hybrid simulation errors for Case 2 are shown in Table 6.

It is shown that for train vehicle model, the peak value errors, the root mean square deviations, and the correlation coefficients of displacement responses at the mid span of the bridge, vertical displacements at the first coupling point, vehicle body displacements, and bogie displacements are less than 25%, less than 0.3031, and more than 0.9566, respectively. The results indicate the calculation accuracy of the hybrid simulation for train vehicle model. Considering the simulation accuracy and test feasibility, the train vehicle the RTHS.As can be seen in Fig .17, the error amplitude of vertical displacement at the first coupling point is 0.16 mm. The error is inevitable due to actuator control. However, the RMSD of vertical displacement at the first coupling point is 0.0777 and the CC is 0.9987. It is shown that the overall trend of hybrid simulation is in good agreement with referenced results.

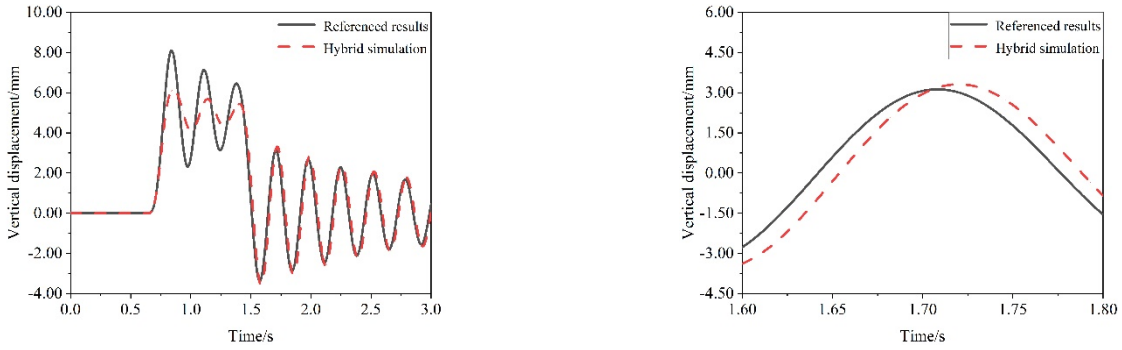

(a) Overall view (b) Close-up view

Fig. 16 Displacement responses at mid span of bridge for Case 2

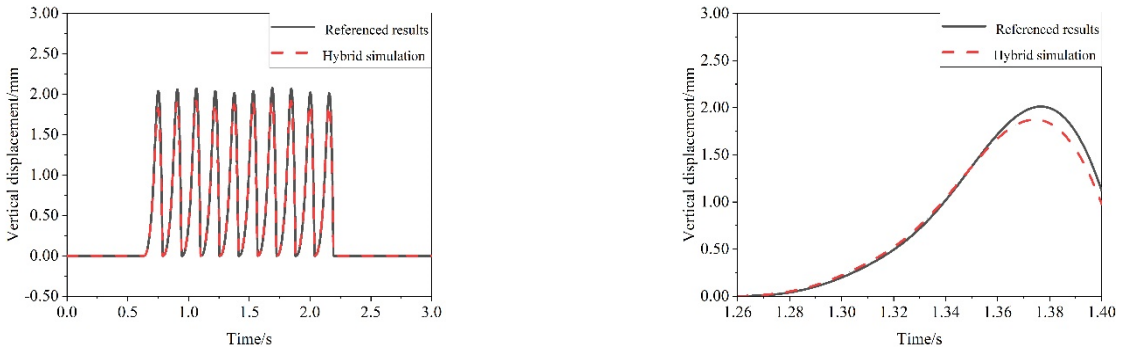

(a) Overall view (b) Close-up view

Fig. 17 Comparison of vertical displacements at the first coupling point for Case 2

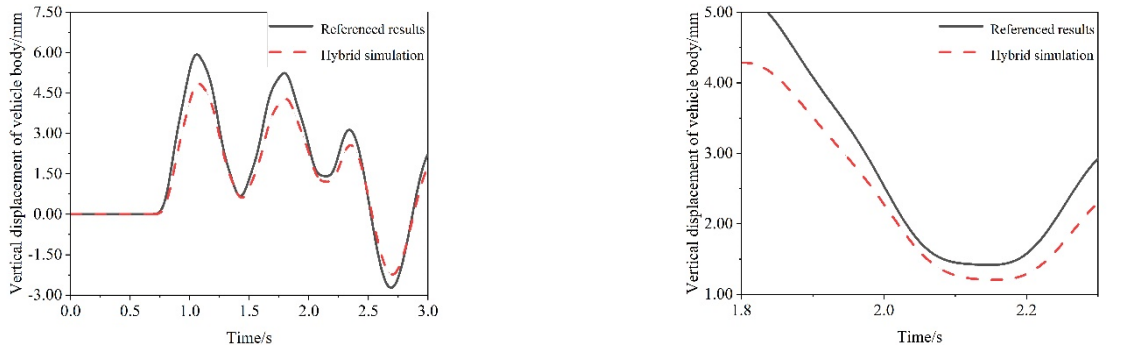

(a) Overall view (b) Close-up view

Fig. 18 Comparison of vertical displacement of vehicle body for Case 2

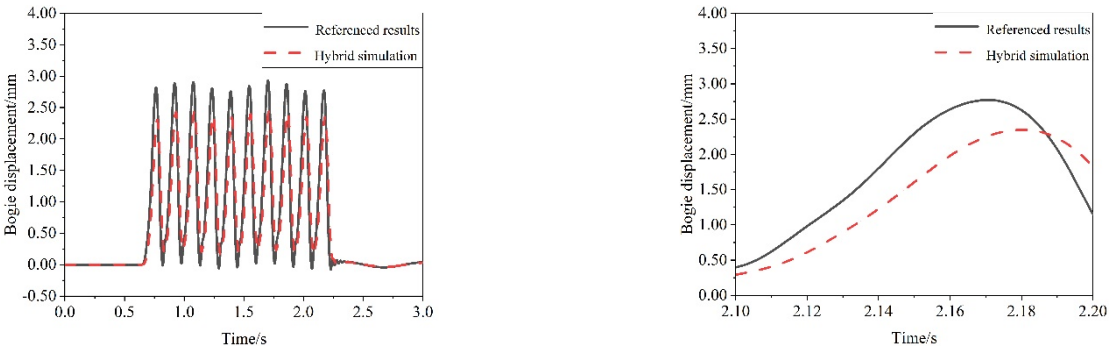

(a) Overall view (b) Close-up view

Fig. 19 Comparison of bogie displacements for Case 2

As can be seen in Table 6, the PVE of bogie displacement is 30.31%. The peak points require higher loading speed, while the defined actuator model is not sufficient to achieve this speed, so as to the PVE and RMSD reached 24.2% and 30.31% whilst overall trend of the hybrid simulation results is in good agreement with the referenced results. The higher frequency of the transfer function of actuator, the less the errors. The index errors are mainly caused by the loading control errors of the actuator system, e.g., the amplitude error and the phase error.

It should be mentioned that the proposed RTHT-VBCS method in this paper only selects the part with complex dynamic performance as the experimental substructure loaded in the laboratory and selects the others as the numerical substructure simulated in one computer, which could greatly save time, labor as well as experimental costs.

Therefore, the economic property of the RTHT-VBCS can be demonstrated.

5. Conclusions

This paper proposed a real-time hybrid testing method for vehicle-bridge coupling systems (RTHT-VBCS) and verified the effectiveness of the proposed method by hybrid simulations. Specifically, the theory of the RTHT-VBCS were proposed, the numerical models for RTHT-VBCS were presented, and the effectiveness and accuracy of the proposed RTHT-VBCS were validated by real-time hybrid simulations (RTHSs). The main conclusions are summarized as follows.

(1) The principle and the test system of RTHT-VBCS was proposed. In the proposed method, one of the carriages is chosen as the experimental substructure loaded by servo-hydraulic actuator loading system in the laboratory, and the remaining carriages as well as the bridge structure are chosen as the numerical substructure numerically simulated in one computer. The numerical substructure and the experimental substructure are synchronized at their coupling points in terms of force equilibrium and deformation coordination. Compared to the traditional iteration experimental method and the numerical simulation method, the proposed RTHT-VBCS could not only obtain the dynamic response of the VBCS, but also economically analyze various working conditions, which indicates the feasibility and advantages of the proposed RTHTVBCS.

(2) The numerical models of vehicle, bridge, and pavement unevenness for RTHS were presented. It is shown that these models can effectively present the VBCS for RTHS in terms of the force equilibrium and deformation compatibility at the coupling points. The hybrid simulation results prove the credibility of the numerical models, i.e., the single-degree-of-freedom and the train vehicle models.

(3) Hybrid simulation scheme of the RTHT-VBCS was presented, and through which the effectiveness and accuracy of the RTHT-VBCS was validated. The single-degree-of-freedom model and the train vehicle model were considered in the hybrid simulations and the corresponding results are compared with the referenced results. It is shown that for the single-degree-of-freedom vehicle model, the results of hybrid simulation match well with the referenced results. Generally speaking, the peak value errors, the root mean square deviations, and the correlation coefficients of dynamic responses at the mid span of the bridge and actuator responses are less than 2%, less than 0.1, and more than 0.99, respectively. It is shown that for the train vehicle model, the results of hybrid simulation almost match the referenced results. Generally speaking, the peak value errors, the root mean square deviations, and the correlation coefficients of displacement responses at the mid span of the bridge, vertical displacements at the first coupling point, vehicle body displacements, and bogie displacements are less than 25%, less than 0.3031, and more than 0.9566, respectively. The hybrid simulation results prove the effectiveness and accuracy of the RTHT-VBCS.

It should be mentioned that in order to further verify the feasibility and effectiveness of the proposed method, the experimental verification should be carried out, and the specific details will be presented in the following paper.

Acknowledgments

The National Natural Science Foundation of China (Grant Nos. 52078150, 51978213, 51908231) and the National Key Research and Development Program of China (Grant Nos. 2017YFC0703605, 2016YFC0701106) are greatly acknowledged for supporting the investigation of this paper.

References

Ahmadizadeh, M., Mosqueda, G. and Reinhorn, A.M. (2008), "Compensation of actuator delay and dynamics for real-time hybrid structural simulation", *Earthq. Eng. Struct. Dyn.*, **37**(1), 21-42. https://doi.org/10.1002/eqe.743

Avci, M., Botelho, R.M. and Christenson, R. (2020), "Real-time hybrid substructuring of a base isolated building considering robust stability and performance analysis", *Smart Struct. Syst., Int. J.*, **25**(2), 155-167. https://doi.org/10.12989/sss.2020.25.2.155

Cai, Y., Chen, S.S., Rote, D.M. and Coffey, H.T. (1996), "Vehicle/Guideway dynamic interaction in maglev systems", *J. Dyn. Sys. Meas. Control*, **118**(3), 526-530. https://doi.org/10.1115/1.2801176

Carrion, J.E., Spencer Jr, B.F. and Phillips, B.M. (2009), "Real-time hybrid simulation for structural control performance assessment", *Earthq. Eng. Eng. Vib.*, **8**(4), 481-492. https://doi.org/10.1007/s11803-009-9122-4

Castaneda, N., Gao, X. and Dyke, S. (2012), "A real-time hybrid simulation platform for the evaluation of seismic mitigation in building structures", *Proceedings of the 20th Analysis and Computation Specialty Conference*, Chicago, IL, USA.

Chen, P.C. and Chen, P.C. (2020), "Robust stability analysis of real-time hybrid simulation considering system uncertainty and delay compensation", *Smart Struct. Syst., Int. J.*, **25**(6), 719-732. https://doi.org/10.12989/sss.2020.25.6.719

Chen, C., Ricles, J.M., Karavasilis, T.L., Chae, Y. and Sause, R. (2012a), "Evaluation of a real-time hybrid simulation system for performance evaluation of structures with rate dependent devices subjected to seismic loading", *Eng. Struct.*, **35**, 71-82. https://doi.org/10.1016/j.engstruct.2011.10.006

Chen, C., Ricles, J.M. and Guo, T. (2012b), "Improved adaptive inverse compensation technique for real-time hybrid simulation", *J. Eng. Mech.*, **138**(12), 1432-1446. https://doi.org/10.1061/(ASCE)EM.1943-7889.0000450

Duvnjak, I., Bartolac, M., Damjanović, D. and Košćak, J. (2020), "Performance assessment of a concrete railway bridge by diagnostic load testing", *Struct. Concrete*, **21**(6), 2363-2376. https://doi.org/10.1002/suco.201900491

Guo, W., Zeng, C., Gou, H., Gu, Q., Wang, T., Zhou, H., Zhang, B. and Wu, J. (2021), "Real-time hybrid simulation of high-speed train-track-bridge interactions using the moving load convolution integral method", *Eng. Struct.*, **228**, 111537. https://doi.org/10.1016/j.engstruct.2020.111537

Guo, W., Long, Y., He, C., Wang, Y., Zeng, Y. and Song, J. (2022), "Off-line hybrid simulation method on train–track–bridge coupling vibration in high-speed railway", *Int. J. Struct. Stab. Dyn.*, **22**(10), 2241014. https://doi.org/10.1142/S0219455422410140

Hayati, S. and Song, W. (2017), "An optimal discrete-time feedforward compensator for real-time hybrid simulation", *Smart Struct. Syst., Int. J.*, **20**(4), 483-498. https://doi.org/10.12989/sss.2017.20.4.483

Horiuchi, T., Inoue, M., Konno, T. and Namita, Y. (1999), "Real-time hybrid experimental system with actuator delay compensation and its application to a piping system with energy absorber", *Earthq. Eng. Struct. Dyn.*, **28**(10), 1121-1141. https://doi.org/10.1002/(SICI)1096-9845(199910)28:10<1121::AID-EQE858>3.0.CO;2-O

Lee, J.S., Kwon, S.D., Kim, M.Y. and Yeo, I.H. (2009), "A parametric study on the dynamics of urban transit maglev vehicle running on flexible guideway bridges", *J. Sound Vib.*, **328**(3), 301-317. https://doi.org/10.1016/j.jsv.2009.08.010

Mahmoud, H.N., Elnashai, A.S., Spencer Jr, B.F., Kwon, O.S. and Bennier, D.J. (2013), "Hybrid simulation for earthquake response of semirigid partial-strength steel frames", *J. Struct. Eng.*, **139**(7), 1134-1148. https://doi.org/10.1061/(ASCE)ST.1943-541X.0000721

Meng, D., Xiao, F., Zhang, L., Xu, X., Chen, G.S., Zatar, W. and Hulsey, J.L. (2019), "Nonlinear vibration analysis of vehicle–bridge interaction for condition monitoring", *J. Low Freq. Noise Vib. Active Control*, **38**(3-4), 1422-1432. https://doi.org/10.1177/1461348418811703

Min, D.J., Jung, M.R., Kim, M.Y. and Kwark, J.W. (2017), "Dynamic interaction analysis of maglev-guideway system based on a 3D full vehicle model", *Int. J. Struct. Stab. Dy.*, **17**(01), 1750006. https://doi.org/10.1142/S0219455417500067

Momoya, Y., Takahashi, T. and Nakamura, T. (2016), "A study on the deformation characteristics of ballasted track at structural transition zone by multi-actuator moving loading test apparatus", *Transp. Geotech.*, **6**, 123-134. https://doi.org/10.1016/j.trgeo.2015.11.001

Muthalif, A.G., Kasemi, H.B., Nordin, N.D., Rashid, M.M. and Razali, M.K.M. (2017), "Semi-active vibration control using experimental model of magnetorheological damper with adaptive F-PID controller", *Smart Struct. Syst., Int. J.*, **20**(1), 85-97. https://doi.org/10.12989/sss.2017.20.1.085

Nakashima, M. and Masaoka, N. (1999), "Real-time on-line test for MDOF systems", *Earthq. Eng. Struct. Dyn.*, **28**(4), 393-420. https://doi.org/10.1002/(SICI)1096-9845(199904)28:4%3C393::AID-EQE823%3E3.0.CO;2-C

Nakashima, M., Kato, H. and Takaoka, E. (1992), "Development of real-time pseudo dynamic testing", *Earthq. Eng. Struct. Dyn.*, **21**(1), 79-92. https://doi.org/10.1002/eqe.4290210106

Ning, X., Wang, Z., Zhou, H., Wu, B., Ding, Y. and Xu, B. (2019), "Robust actuator dynamics compensation method for real-time hybrid simulation", *Mech. Syst. Signal Process*, **131**, 49-70. https://doi.org/10.1016/j.ymssp.2019.05.038

Ou, G., Ozdagli, A.I., Dyke, S.J. and Wu, B. (2015), "Robust integrated actuator control: experimental verification and real-time hybrid-simulation implementation", *Earthq. Eng. Struct. Dyn.*, **44**(3), 441-460. https://doi.org/10.1002/eqe.2479

Pawlus, W., Karimi, H.R. and Robbersmyr, K.G. (2011), "Mathematical modeling of a vehicle crash test based on elasto-plastic unloading scenarios of spring-mass models", *Int. J. Adv. Manuf. Technol.*, **55**(1), 369-378. https://doi.org/10.1007/s00170-010-3056-x

Phillips, B.M., Wierschem, N.E. and Spencer Jr, B.F. (2014), "Model-based multi-metric control of uniaxial shake tables", *Earthq. Eng. Struct. Dyn.*, **43**(5), 681-699. https://doi.org/10.1002/eqe.2366

Schellenberg, A.H., Mahin, S.A. and Fenves, G.L. (2009a), Advanced Implementation of Hybrid Simulation; PEER Report 2009-104. Pacific Earthquake Engineering Research Center, University of California, Berkeley, CA, USA.

Schellenberg, A.H., Kim, H.K., Takahashi, Y., Fenves, G.L. and Mahin, S.A. (2009b), Open Fresco Command Language Manual; The Regents of the University of California, Berkeley, CA, USA.

Shao, X., Mueller, A. and Mohammed, B.A. (2016), "Real-time hybrid simulation with online model updating: methodology and implementation", *J. Eng. Mech.*, **142**(2), 04015074. https://doi.org/10.1061/(ASCE)EM.1943-7889.0000987

Shao, P., Guo, W., Lei, Q. and Zeng, C. (2021), "Adaptive compound control for the real–time hybrid simulation of high–speed railway train–bridge coupling vibration", *Struct. Control Health Monitor.*, **28**(11), e2816. https://doi.org/10.1002/stc.2816

Shi, X., Zou, X. and Yang, P. (2010), "Study on road simulation test of motorcycle", *Appl. Mech. Mater.*, **29-32**, 1556-1561. https://doi.org/10.4028/www.scientific.net/AMM.29-32.1556

Tan, C. and Uddin, N. (2020), "Hilbert transform based approach

to improve extraction of "drive-by" bridge frequency", *Smart Struct. Syst., Int. J.*, **25**(3), 265-277. https://doi.org/10.12989/sss.2020.25.3.265

Tang, Z., Gao, F., Liu, H. and Li, Y. (2023), "Implementation of shaking table based offline hybrid simulation through neural networks", In: *Structures*, Vol. 48, pp. 21-30. https://doi.org/10.1016/j.istruc.2022.12.050

Wang, T., Huang, D. and Shahawy, M.A. (1992), "Dynamic response of multigirder bridges", *J. Struct. Eng.*, **118**(8), 2222-2238. https://doi.org/10.1061/(ASCE)0733-9445(1992)118:8(2222)

Wang, Z., Ning, X., Xu, G., Zhou, H. and Wu, B. (2019), "High performance compensation using an adaptive strategy for real-time hybrid simulation", *Mech. Syst. Signal Process*, **133**, 106262. https://doi.org/10.1016/j.ymssp.2019.106262

Wang, Z., Xu, G., Li, Q. and Wu, B. (2020), "An adaptive delay compensation method based on a discrete system model for real-time hybrid simulation", *Smart Struct. Syst., Int. J.*, **25**(5), 569-580. https://doi.org/10.12989/sss.2020.25.5.569

Wu, B., Xu, G., Wang, Q. and Williams, M.S. (2006), "Operator-splitting method for real-time substructure testing", *Earthq. Eng. Struct. Dyn.*, **35**(3), 293-314. https://doi.org/10.1002/eqe.519

Wu, B., Wang, Q., Benson Shing, P. and Ou, J. (2007), "Equivalent force control method for generalized real-time substructure testing with implicit integration", *Earthq. Eng. Struct. Dyn.*, **36**(9), 1127-1149. https://doi.org/10.1002/eqe.674

Wu, B., Deng, L. and Yang, X. (2009), "Stability of central difference method for dynamic real-time substructure testing", *Earthq. Eng. Struct. Dyn.*, **38**(14), 1649-1663. https://doi.org/10.1002/eqe.927

Xi, R., Chen, Q., Meng, X. and Jiang, W. (2017), "Analysis of bridge deformations using real-time BDS measurements", *Proceedings of the 6th International Conference on Computer Science and Network Technology*, Dalian, China, October.

Xu, G., Wang, Z., Bao, Y., Yang, G. and Wu, B. (2020), "Shaking table substructure testing based on three-variable control method with velocity positive feedback", *Appl. Sci.*, **10**(16), 5414. https://doi.org/10.3390/app10165414

Xu, G., Zheng, L. and Bao, Y. (2022), "Shaking table substructure test of tuned liquid damper for controlling earthquake response of structure", *Struct. Control Health Monit.*, **29**(12), e3122. https://doi.org/10.1002/stc.3122

Yang, Y.B., Lin, C.W. and Yau, J.D. (2004), "Extracting bridge frequencies from the dynamic response of a passing vehicle", *J. Sound Vib.*, **272**(3-5), 471-493. https://doi.org/10.1016/S0022-460X(03)00378-X

Yang, T.Y., Stojadinovic, B. and Moehle, J. (2009), "Hybrid simulation of a zipper-braced steel frame under earthquake excitation", *Earthq. Eng. Struct. Dyn.*, **38**(1), 95-113. https://doi.org/10.1002/eqe.848

Zhou, H., Xu, D., Shao, X., Ning, X. and Wang, T. (2019), "A robust linear-quadratic-gaussian controller for the real-time hybrid simulation on a benchmark problem", *Mech. Syst. Signal Process.*, **133**, 106260. https://doi.org/10.1016/j.ymssp.2019.106260